17th World Conference on Earthquake Engineering, 17WCEE

Sendai, Japan - September 13th to 18th 2020

UNDERSTANDING THE IMPLICATIONS OF SEISMICITY INDUCED BY UK SHALE GAS DEVELOPMENT

G. Cremen[(1)], M.J. Werner[(2)], B. Baptie[(3)]

[(1)] *Research Fellow, University College London, cremengem@gmail.com*
[(2)] *Senior Lecturer, University of Bristol, max.werner@bristol.ac.uk*
[(2)] *Seismologist, British Geological Survey, bbap@bgs.ac.uk*

Abstract

Shale gas development can be a source of concern for local populations and stakeholders, as the associated process of hydraulic fracturing may be accompanied by microseismicity and – in some locations – small to moderate seismic events with ground motions that have the potential to be felt (i.e., cause a nuisance) nearby. The purpose of this study is to help quantify this nuisance potential. We specifically focus on the UK, where shale gas development is a relatively new industrial activity; the first well to specifically test for shale gas in the country was drilled in 2010 and the first recorded instance of seismicity induced by hydraulic fracturing in the UK occurred in 2011. We propose a novel framework for quantifying the hydraulic-fracture-related nuisance risk, and apply it to the Preston New Road (PNR) shale gas site in Lancashire, North West England, where hydraulic fracture operations in 2018 and 2019 resulted in events with local magnitude range (M_L) -1.7 to 2.9, including eight that were felt by local populations. The framework is a modified version of probabilistic seismic hazard analysis (PSHA) that combines statistical forecast models for injection-induced seismicity, ground motion prediction equations (GMPEs), and an exposure model of the affected area, to quantitatively link the volume of fluid injected with the potential for nuisance felt ground motions. For the greater PNR region, we find that ground motions equivalent in amplitude to that at which pile driving becomes perceptible may be exceeded in the location of at least one building for event magnitudes equal to or exceeding the current UK induced seismicity traffic light system "red light" event (i.e $M_L = 0.5$), or injection volumes ≥ 1000 m^3. We also find that cosmetic damage may occur in at least one building for $M_w \geq 2.1$ or injection volumes $\geq 40{,}000$ m^3. The proposed nuisance risk quantification framework is proactive in nature, as it facilitates control of the injection volume ahead of time for risk mitigation. This type of framework has significant advantages over reactive-type magnitude and ground motion-based systems typically used for induced seismicity management. We also discuss how the proposed framework can be used to inform policy related to hydraulic-fracture induced seismicity. This research is intended to help stakeholders make better-informed decisions about the regulation of shale gas development in the UK and other countries.

Keywords: Induced seismicity; Hydraulic fracturing; Seismic hazard; Felt ground motions; Nuisance risk

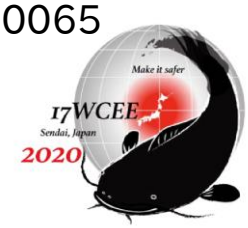

1. Introduction

Awareness and concern regarding the impacts of seismicity induced by hydraulic fracturing has grown significantly in recent years [e.g. 1,2], which may pose a threat to the future development of unconventional gas resources [3]. There is evidence that tolerance to such operations will be increased if the public is made aware of the potential consequences of the resulting ground shaking [4,5]. In addition, understanding these consequences is critical for responsible decision-making by relevant political authorities [6]. It is therefore essential to develop methodologies for quantifying and managing the hazard and risk posed by hydraulic-fracture induced seismicity.

Several hazard and risk assessment procedures have already been proposed in the literature for various types of induced seismicity. For example, Douglas and Aochi [7] developed a conceptual model for assessing the risk of generating felt or damaging ground motions from enhanced geothermal systems (EGS), based on fluid injection rate. It used information on recent seismicity and ground shaking predictions from a GMPE to obtain a real-time hazard curve, which was combined with a fragility curve to quantify risk. Gupta and Baker [8] developed a probabilistic framework for estimating regional risk due to induced seismicity related to wastewater injection in Oklahoma that extends conventional probabilistic seismic hazard analysis to account for spatiotemporally varying seismicity rates. Walters et al. [9] developed a qualitative risk assessment framework for triggered seismicity related to saltwater disposal and hydraulic fracturing that included risk tolerance matrices to be considered by different stakeholders.

This paper proposes a novel risk assessment framework for hydraulic-fracture induced seismicity that directly links the volume of fluid injected during an operation to its potential for causing nuisance ground motions, i.e. shaking that may raise annoyance or distress among the public [10]. This type of shaking is expected to be more in line with public tolerances for induced seismicity than larger ground motions that have the potential to cause structural damage [4]. The framework integrates, in a mathematically rigorous manner, statistical forecast models for injection-induced seismicity, ground motion prediction equations for hydraulic fracturing, and exposure models for nearby areas.

The framework is applied to the region surrounding the PNR shale gas site in Lancashire, North West England, where recent hydraulic fracture operations resulted in 29 seismic events with M_L greater than 0, including eight that were felt by the local population. We demonstrate how the risk calculations can accommodate different styles of potential decision-making related to the regulation of hydraulic-fracture-induced seismicity. The paper ends with a discussion on ways in which the proposed framework could be used to design future policies related to the management of hydraulic-fracture-induced risk in the UK.

2. Framework Outline

The proposed framework is a modified version of PSHA [11], where the rate of earthquake occurrence, the distribution of magnitudes, and therefore the rate of exceedance for a given intensity measure (*IM*), are conditioned on the total volume of fluid injected during a hydraulic fracture operation (V_t). It may be expressed as follows:

$$\lambda(IM > x|V_t) = \sum_i^s \lambda(M_s > m_{min}|V_t) \; \left[\int_{m_{min}}^{m_{max}|V_t} \int_0^{r_{max}} p(IM > x|m,r) f_{M|V_t}(m) f_R(r) \, dm \, dr\right] \quad (1)$$

where *s* is the number of earthquake sources, $\lambda(a > b|c)$ is the is the rate at which a exceeds b given the occurrence of *c*, *p(k|j)* is the probability of *k* given *j*, m_{min} is the minimum magnitude considered, $m_{max}|V_t$ is the maximum magnitude considered for a given injection volume, $f_Y(y)$ is the probability density function of *Y* evaluated at *y*, and *r* is the distance from the source to the location of interest.

The "$\lambda(M_s > m_{min}|V_t)$" and "$f_{M|V_t}(m)$" terms are characterized by a statistical forecast model for injection-induced seismicity, the "$p(IM > x|m,r)$" term is derived from ground shaking estimations by a GMPE designed for hydraulic fracturing events, and the "$f_R(r)$" term is obtained from an exposure model of the affected region. While the framework is sufficiently flexible to cater for any intensity measure, we

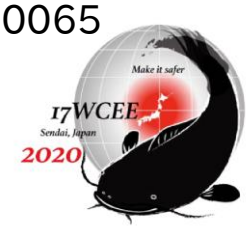

specifically use Peak Ground Velocity (*PGV*) as the measure of ground shaking in this study (i.e. *IM* = *PGV* in equation Eq. (1)) because of its close correlation with seismic intensity [12] and its ability to indicate damage for the small, shallow earthquakes of interest in this study [13].

The framework is based on the assumption of a one-to-one relationship between the exceedance of tolerable ground shaking thresholds and nuisance risk, i.e.

$$p(NR_i|im > x_i) = 1 \quad (2)$$

where NR_i is the nuisance risk associated with the *i*th tolerable ground shaking threshold, x_i. Tolerance for potential ground shaking may be dependent on the culture of those affected [10], and a discussion with local stakeholders is therefore necessary to decide exactly what risk is acceptable [5]. However, our methodology provides a number of suggested tolerable ground shaking thresholds, based on previous studies associated with discomfort due to ground [14] and nuisance limits adopted for other types of vibration. These are: (1) *PGV* = 0.9 mm/s, which approximately corresponds with the velocity at which pile driving becomes `barely perceptible' [15]; (2) *PGV* = 3 mm/s, which is the velocity at which traffic-induced vibration becomes `barely noticeable' [16]; (3) *PGV* = 15 mm/s, which is the lowest threshold of cosmetic damage for weak (i.e. unreinforced or light framed) structures, according to the British Standards Institute (BSI) [17] and has been used in previous risk calculations for induced seismicity [18]; and (4) *PGV* = 50 mm/s, which is the BSI [17] threshold of cosmetic damage for strong (i.e. reinforced or framed) structures.

3. Case Study Framework Application

We apply the proposed framework to the region surrounding the PNR shale gas site in Lancashire, North West England, where hydraulic fracturing operations took place in late 2018 (at PNR-1z well) and mid 2019 (at PNR-2 well), resulting in a number of felt seismic events with maximum magnitude M_L = 2.9. For the purposes of this application, we assume that seismicity is produced from a point source 2 km deep (i.e. *n*=1 in Eq. (1)) at a respective latitude and longitude of 53.7873º North and 2.9511º West. This location corresponds to the approximate depth of the Bowland shale targeted by the operation and the surface coordinates of the PNR-1z well, according to the 2018 hydraulic fracture plan of the operator [19].

3.1 Source and Ground Motion Modeling

We use the Hallo et al. [20] injection-volume-based statistical model of event magnitudes, as it was used for real-time seismicity forecasting by the operator during hydraulic fracturing at PNR [21]. This model assumes that the cumulative seismic moment released M_o is related to the total volume of fluid injected (V_t) as follows:

$$\sum M_o = S_{EFF}\mu V_t \quad (3)$$

where μ is the rock shear modulus. S_{EFF} depends on the rock type and the nature of the injected material, and represents the ratio of $\sum M_o$ to its theoretical maximum (μV_t) assuming no aseismic deformation [22]. For this formulation:

$$\sum_j^n M_{jo} \leq \sum M_o \quad (4)$$

where M_{jo} is the seismic moment equivalent of the *j*th earthquake and *n* is the number of earthquakes that occur, which is a random variable that follows a Poisson probability mass function with mean $N = \sum_i^s \lambda(M_s > m_{min}|V_t)$ from Eq. (1). $m_{max}|V_t$ in equation Eq. (1) for the *i*th event is defined as:

$$m_{max}|V_t = \alpha_{i-1} \sum M_{o,w} \quad (5)$$

where α_{i-1} is the fraction of $\sum M_{o,w}$, the total seismic moment in moment magnitude terms, still to be released after the occurrence of the (*i-1*)th event.

μ is assumed to be 20 GPa throughout this study, from previous work on PNR seismicity [21]. The sets of S_{EFF}, m_{min} and *b*- values used are those fit by Clarke et al. [21] for seismicity produced during PNR-1z

operations, where 17 sleeves were stimulated with a total injection volume of approximately 4200 m^3. We treat the stimulated sleeves before Sleeve 18 (i.e. Sleeves 1, 2, 3, 12, 13, and 14) as independent, and use the relevant set of sleeve-specific seismicity parameters for each. For the 11 remaining stimulated sleeves, we use the set of seismicity parameters fit over their cumulative injected volume, as they were found to intersect the same fault [21]. It should be noted that some sets of seismicity parameters used were fit using a mixture of event magnitudes reported on moment and local scales [21], yet the size of forecasted events are always measured on the moment magnitude scale. This discrepancy is deemed acceptable however, given that the precise relationship between the scales is yet to be established [23].

Ground shaking ($p(IM > x|m,r)$ in Eq. (1)) is predicted using the ground motion prediction equation of Cremen at al. [24], which was specifically designed for hydraulic-fracture induced seismicity in the UK. This equation characterises ground motion intensity in terms of moment magnitude and hypocentral distance at the location of interest. It is intended to model ground motion amplitudes for events with M_w < 3 at hypocentral distances < 6 km.

3.2 Exposure Database

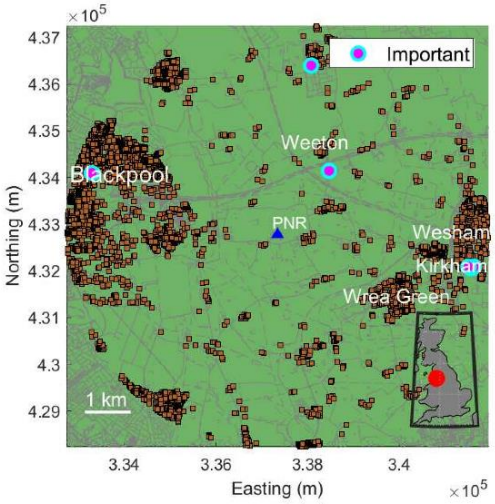

Fig. 1 – All buildings (brown squares) and important (i.e. educational and medical) buildings considered within 5 km hypocentral distance of the case study event location at the PNR hydraulic fracture site (inset highlights location relative to all of Great Britain).

The considered exposure database ($f_R(r)$ in Eq. (1)) comprises buildings located within a 5 km hypocentral distance of the event location (Fig. 1). Building data are obtained from Ordnance Survey (OS) mapping, accessed through the Edina Digimap service [24]. Building footprint information is acquired from the 'Buildings' layer of the OS VectorMap Local product, and building height information is acquired from the OS MasterMap `Building Height Attribute' database. Height and footprint data are matched via their geographic coordinates; we consider the corresponding building height for a given building footprint to be the closest located within 10 m. To exclude small non-habitable structures, we neglect buildings with footprint areas < 40 m^2 and/or known building heights < 3.5 m. This results in a final exposure database of 4195 buildings.

We also separately consider important buildings, in which the occupants (or equipment) may be more sensitive to the effects of vibrations from ground shaking than those of conventional residential or commercial buildings [9, 18]. We exclusively focus on educational and medical facilities within 5 km of the event, which are identified from the `Important Buildings' layer of the OS VectorMap Local. We neglect all important buildings with footprint areas < 100 m, which is the typical size of a classroom [26]. This results in a final database of six important buildings.

3.3 Monte Carlo Sampling Procedure

Eq. (1) describes ground motion exceedance at a single site. To capture the risk across the multiple sites of interest in this study and correctly account for ground motion variability [27], we employ a Monte Carlo sampling approach [28]. This procedure involves the following steps for a given injection volume:

1. Calculate the corresponding total seismic moment, using Eq (3).
2. Choose a single random event from the magnitude distribution $f_{M|Vt}(m)$ of Eq. (1), which is truncated on the left by m_{min} and on the right by $m_{max,i}|V_t$ (as defined in Eq. (5)).
3. Use the Cremen et al. GMPE [24] to simulate a random inter-event variability and random intra-event variabilities for each site.
4. Calculate median ground motion predictions from the GMPE at each site for the given combination of $\{m,r\}$, and add the inter- and intra-event variabilities generated in step 3 to simulate ground motion intensities.
5. Repeat Step 2-4 until the total seismic moment of the sampled events is equal to that calculated in step 1 to within a small tolerance.
6. Repeat Steps 2-5 1000 times to generate 1000 potential catalogs corresponding to the given injected volume.

3.4 Modeling Validation

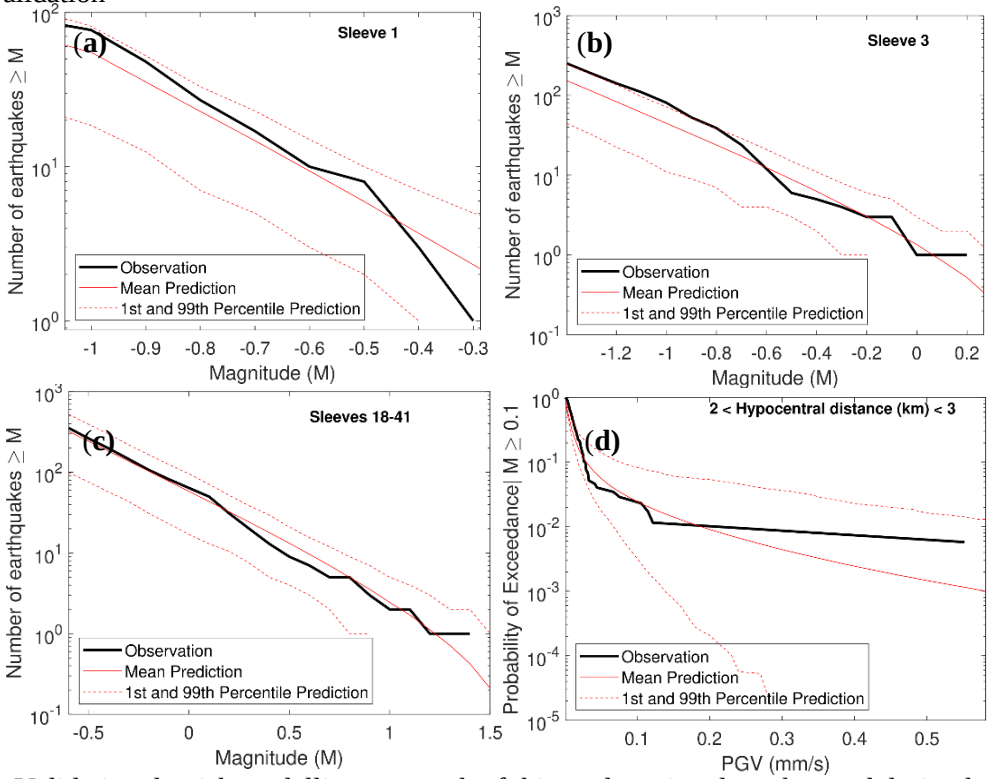

Fig. 2 – Validating the risk modelling approach of this study, using data observed during hydraulic fracturing of the PNR 1-z well: (a)-(c) Comparing forecasted numbers of earthquakes with those observed; and (d) Comparing predicted ground shaking with observed ground motion amplitudes.

The proposed risk modelling approach is validated using data observed during the 2018 hydraulic fracturing operations at the PNR 1-z well. We complete the Monte Carlo sampling procedure for the actual volumes of fluid injected during those operations, using the UK Oil and Gas Authority's database on PNR operations (https://www.ogauthority.co.uk/onshore/onshore-reports-and-data/preston-new-road-pnr-1z-hydraulic-fracturing-operations-data/). Figs. 2a-2c compare the predicted numbers of earthquakes with those observed across selected sleeves (similar results are obtained for the remaining sleeves).

It is seen that the observations almost always lie within the 1st and 99th percentile predictions of the model, thus we can conclude that the source model used is appropriate for forecasting the seismicity of interest.

Fig. 2d compares ground shaking predictions at locations in the exposure model with observed ground motion amplitudes, for all forecasted/recorded events of $M_w \gtrapprox 0.1$, within a 2-3 km hypocentral distance range. This distance range is chosen since it corresponds to: (1) a similar number of predictions (229 per synthetic catalog) and observations (173); and (2) an almost identical mean hypocentral distance for predictions (2.66 km per synthetic catalog) and observations (2.69 km). It is seen that the observed ground shaking amplitudes generally lie within the 1st and 99th percentile predictions, and therefore it is clear that the proposed model is adequately capturing the shaking intensity (risk) of interest. This confirms that the slight magnitude scale discrepancy in the source model (see Section 3.1) does not inhibit the overall performance of the calculations.

4. Case Study Results

4.1 Magnitude-Specific Calculations

We first examine the risk associated with the occurrence of specific moment magnitudes (M_w) up to $M_w = 3.0$, which is the maximum applicable magnitude for the Cremen et al. [24] GMPE. We repeat steps 3 and 4 of Section 3.3 1000 times for M_w between 0.1 and 3, in increments of 0.1. Results of the calculations are found in Fig. 3, where they are presented three different ways to accommodate various potential styles of decision-making. Fig. 3a-3d summarize the probability of exceeding the prescribed risk thresholds at least once across different magnitude-distance bins, considering all buildings.

As expected, the probability of exceeding the thresholds increases for increasing magnitude and decreasing hypocentral distance. It is observed that the $PGV = 0.9$ mm/s (pile driving perceptibility) threshold exceedance probability becomes non-zero for $M_w \gtrapprox 1.1$ at close distances, and for $M_w \gtrapprox 1.8$ at all examined distances. The $PGV = 3$ mm/s (traffic noticeable) threshold exceedance probability becomes non-zero for $M_w \gtrapprox 1.6$ and non-zero at all examined distances for $M_w \gtrapprox 2.3$. The $PGV = 15$ mm/s (cosmetic damage for weak structures) threshold exceedance probability becomes non-zero for $M_w \gtrapprox 2.1$ and for $M_w \gtrapprox 2.8$ at all distances of interest. The $PGV = 50$ mm/s (cosmetic damage for strong structures) threshold exceedance probability becomes non-zero for $M_w \gtrapprox 2.5$, but does not become non-zero across all examined distances for any magnitude of interest in this study.

Fig. 3e and Fig. 3f examine the risk associated with three specific magnitudes: (1) $M_L = 0.5$, which is the current red light ("stop injection") threshold for hydraulic-fracture-induced seismicity in the UK, (2) $M_L = 2.1$, which was the second-largest event that occurred during 2018/2019 PNR operations, and (3) $M_L = 2.9$, which was the largest event that occurred during 2018/2019 PNR operations. These magnitudes are converted to moment magnitude for input to the Cremen et al. [24] GMPE, using the empirical relationship derived by Butcher et al. [29] for small magnitudes in a similar geologic setting; this is an approximate conversion, since the relationship between the scales is uncertain [23]. For this relationship, (1) $M_L = 0.5$ is equivalent to $M_w = 1.1$, (2) $M_L = 2.1$ is equivalent to $M_w = 2.2$, and (3) $M_L = 2.9$ is equivalent to $M_w = 2.7$.

Fig. 3e shows the probability of exceeding different PGV levels at least once, across all considered buildings (magenta curves) and important buildings (blue curves). It is seen that the current red light event for UK hydraulic fracturing has only a negligible probability of exceeding the lowest of the four considered tolerable risk thresholds at the location of at least one building in the exposure model. An event equivalent in size to the second largest 2019 event will almost certainly exceed both the pile driving and traffic thresholds, and has a negligible chance of causing cosmetic damage in a worst case scenario (i.e. weak structure). An event equivalent in size to the largest 2019 event exceeds the first three considered tolerable risk thresholds with certainty, and there is an approximate 10% chance that it will result in ground motions that cause cosmetic damage in a best case scenario (i.e. strong structure). The predicted occurrence of cosmetic damage for $M_w = 2.7$ is consistent with actual observations (despite the hypothetical event being located approximately 0.8 km to the west of where the actual event occurred, at a 0.5 km shallower depth); the British Geological Survey

assigned the event an intensity of 6 on the European Macroseismic Intensity scale [30] meaning "slightly damaging", based on data from more than 2000 felt reports [31].

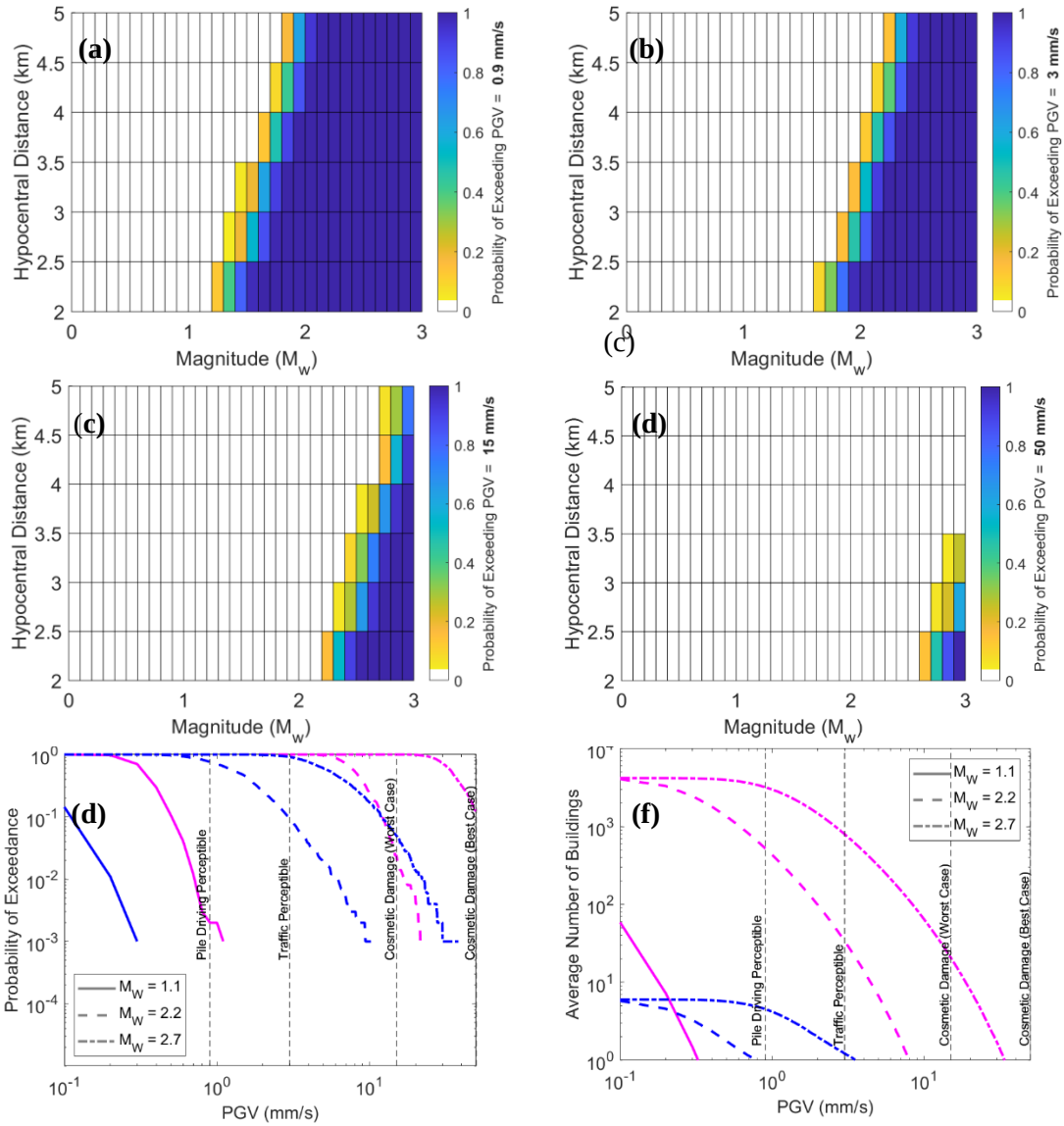

Fig. 3 – Magnitude-specific risk calculations: (a)-(d) summarize the probability of *PGV* exceeding the prescribed risk thresholds (0.9 mm/s, 3 mm/s, 15 mm/s, and 50 mm/s respectively) at least once across different magnitude-distance bins; (e) highlights, for three specific magnitudes, the probability of exceeding various *PGV* levels at least once for all buildings (magenta curves) and important buildings (blue curves); and (f) shows, for three specific magnitudes, the average number of buildings (blue curves) and important buildings (magenta curves) at which various *PGV* levels are exceeded.

It is also seen in Fig. 3e that the curves associated with important buildings are positioned to the left of those associated with all buildings, for the same magnitude event. This implies that the risk for important buildings is lower than that for all buildings. For example in the worst case scenario, there is only approximately 10% probability of cosmetic damage occurring in at least one important building versus near certainty of this type of damage occurring in at least one building, for an event equivalent to the largest that occurred in 2019. The smaller risk associated with important buildings makes sense, since they are located further away from the hydraulic fracture site than the closest of all considered buildings (see Fig. 1).

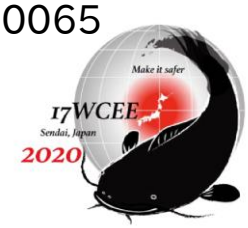

Fig. 3f shows the average number of all buildings (magenta curves) and important buildings (blue curves) at which different *PGV* levels are exceeded for the three specific magnitudes examined. Less than one building is expected to experience shaking that exceeds the lowest of the four considered tolerable risk thresholds, for an event equal in size to the current UK red light event. Approximately 30 buildings are expected to experience ground motions that exceed the traffic threshold for an event equivalent in size to the second largest that occurred in 2019, and approximately 20 buildings are expected to experience cosmetic damage in a worst case scenario for an event equivalent in size to the largest in 2019. In the case of important buildings, less than one is expected to experience exceedance of the pile driving threshold for either M_w = 1.1 or M_w = 2.2, and approximately one is expected to experience exceedance of the traffic threshold for M_w = 2.7.

4.2 Volume-Specific Calculations

We use the procedure outlined in Section 3.3 to examine the risk associated with the following injection volumes: 500 m^3, 1000 m^3, 5000 m^3, 10,000 m^3, 15,000 m^3, 20,000 m^3, 30,000 m^3, 40,000 m^3, and 50,000 m^3. These values capture the typical range of injection volumes planned/used for hydraulic fracturing operations in both the UK [e.g. 19, 32] and North America [e.g. 33, 34]. We assume that each volume is divided evenly among the 17 stimulated sleeves of the PNR-1 operation, and simulate seismicity according to the sleeve-dependent parameters discussed in Section 3. Results of the calculations are summarized in Fig 4, using similar presentation methods as those introduced in Section 4.1.

Figs. 4a-4d show the probability of exceeding the prescribed risk thresholds at least once across different volume-distance bins, considering all buildings. The probability of exceeding the thresholds clearly increases as injection volume increases and hypocentral distance decreases, in line with expectations. It is seen that the *PGV* = 0.9 mm/s (pile driving) threshold exceedance probability becomes non-zero at close distances for 1000 m^3 of injected volume, and at all examined distances for 10,000 m^3. The *PGV* = 3 mm/s (traffic) threshold exceedance probability becomes non-zero for 5000 m^3, and non-zero at all examined distances for 40,000 m^3. The *PGV* = 15 mm/s (cosmetic damage for weak structures) threshold exceedance probability becomes non-zero for 40,000 m^3, but does not become non-zero across all examined distances for any injection volume of interest. The *PGV*=50 mm/s (cosmetic damage for strong structures) threshold is not exceeded for the examined injection volumes.

Fig. 4e and Fig. 4f examine the risk associated with the specific injection volumes of interest, across different *PGV* levels. Fig. 4e shows the probability of exceeding a given value of *PGV* at least once, across all considered buildings (magenta curves) and important buildings (blue curves). It is seen that there is no chance of exceeding any of the considered tolerable risk thresholds for 500 m^3 injected volume, and there is only a negligible probability of exceeding the lowest of the four considered thresholds at least once for 1000 m^3, 5000 m^3, 10,000 m^3, 15,000 m^3, 20,000 m^3, and 30,000 m^3 have approximately 2%, 10%, 30%, 50%, and 80\% chance respectively, of generating ground motions that exceed the traffic threshold at the location of at least one building in the exposure model. The largest two injection volumes considered (i.e. 40,000 m^3 and 50,000 m^3) will almost certainly result in shaking that exceeds the traffic threshold, but will only result in cosmetic damage in a worst case scenario (weak structure) with less than 10% probability. It appears that no injected volumes examined have any chance of causing cosmetic damage in a best case scenario (strong structure). Curves associated with important buildings are positioned to the left of those associated with all buildings in Fig. 4e, implying lower risk for important buildings as discussed in Section 4.1. For example in the worst case scenario, there is negligible chance of cosmetic damage occurring in at least one important building versus approximately 9% probability of this type of damage occurring in at least one building, for the largest considered injected volume.

Fig. 4f shows the average number of all buildings (magenta curves) and important buildings (blue curves) at which different *PGV* levels are exceeded for the injection volumes examined. Less than one important building is expected to experience shaking that exceeds the lowest of the four considered tolerable risk thresholds for any injected volume analyzed, and less than one building of any type is expected to experience exceedance of this threshold for both 500 m^3 and 1000 m^3 injected volumes. Less than 10 buildings are expected to experience exceedance of the lowest threshold for 5000 m^3, and between 10 and 100 buildings

are expected to experience shaking above this threshold for 10,000 m^3, 15,000 m^3, and 20,000 m^3. Between 10 and 100 buildings are expected to experience exceedance of the traffic threshold for the 30,000 m^3, 40,000 m^3, and 50,000 m^3. Less than one building is expected to experience cosmetic damage in a worst case scenario, for any injected volume examined.

It is important to note that the calculations of Section 4 have made a number of assumptions related to the source modelling and prediction of ground motion. For example, it was assumed that all seismicity was co-located and that there were no spatial correlations in the ground motions from a given event. Future studies will critically examine the impact of these assumptions on the results.

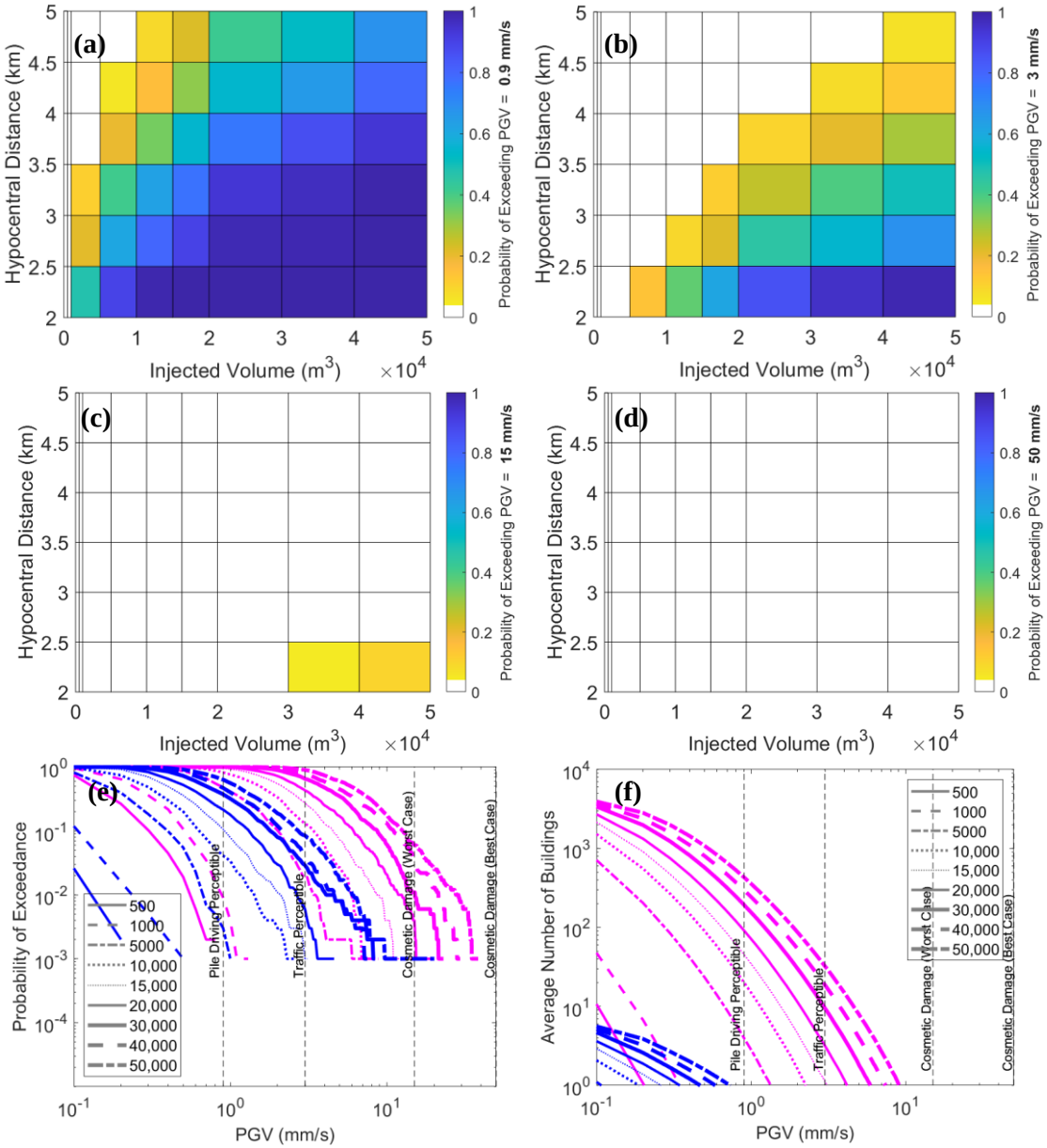

Fig. 4 – Injection-volume-based risk calculations: (a)-(d) summarize the probability of *PGV* exceeding the prescribed risk thresholds (0.9 mm/s, 3 mm/s, 15 mm/s, and 50 mm/s respectively) across different volume-distance bins; (e) highlights, for specific volumes, the probability of exceeding various *PGV* levels at least once for all buildings (magenta curves) and important buildings (blue curves); and (f) shows, for specific volumes, the average number of buildings (magenta curves) and important buildings (blue curves) at which various *PGV* levels are exceeded.

5. Implications for Future Policy Design

The UK Oil and Gas Authority has implemented a magnitude-based traffic light system (TLS) for the management of induced seismicity related to onshore shale gas exploration in the country. This TLS allows operations to continue as planned ("green light") when the related induced seismicity is below M_L =0.0, requires operations to proceed with caution ("amber light") when the seismicity reaches M_L =0.0 to M_L =0.5 and stipulates a halt in operations ("red light") when seismicity with $M_L \geq 0.5$ occurs.

However, such magnitude-based systems have limited connection to the actual risks associated with the induced seismicity; it is instead the intensity of the ground motions [4], in combination with an exposure model of the surrounding region, which determine the probability for nuisance or more damaging consequences. The results presented in Section 4.1 of this study could be used to design a more risk-orientated TLS for induced seismicity related to UK hydraulic fracturing, in which the magnitudes corresponding to each level of the system are chosen based on their potential to lead to ground motions that may cause nuisance consequences in the nearby area. For example, an "amber light" may correspond to the lowest magnitude for which there is a non-zero probability of the pile driving threshold being exceeded at any building (M_w = 1.1 for PNR from Section 4.1 and a "red light" may correspond to a magnitude just below that for which there is a non-zero chance of cosmetic damage occurring at any building in a worst case scenario (M_w = 2.1 for PNR). Similar approaches have been adopted for enhanced-geothermal-induced seismicity [e.g. 14,18], although our study has been informed by a more comprehensive analysis of the nearby exposure.

Alternatively, the proposed framework in Eq. (1) and the results of Section 4.2 could be used to design an injection-volume-based TLS for managing the risk associated with UK hydraulic-fracture-induced seismicity, where each level of the system corresponds to volumes of injected fluid with certain probabilities of causing ground motions that have nuisance potential. For example, an "amber light" could correspond to the first volume for which there is a non-zero probability of the pile driving threshold being exceeded, i.e. 1000 m^3 for PNR from Section 4.2, which is roughly equivalent to a quarter of the actual volume injected during PNR-1z operations [21] and a "red light" could correspond to a volume just less than that for which there is a non-zero chance of cosmetic damage occurring in a worst case scenario, i.e. 40,000 m^3 for PNR, which is approximately equal to the planned injection volume for PNR-2 [32].

A significant advantage of this approach over conventional magnitude- or ground motion-based TLSs is that it is proactive rather than reactive, since the injection volume can be controlled ahead of time to avoid a "red light" ever occurring. However, additional studies are required to understand the sensitivity of the calculations to the modeling assumptions and therefore the amount of a-priori information that would be needed for such a system to perform accurately.

6. Conclusions

This study has presented a novel framework for assessing the consequences of hydraulic-fracture-induced seismicity. The framework explicitly links the volume of fluid injected during operations to the risk of nuisance ground shaking, by combining statistical forecast models for injection-related seismicity, ground motion prediction equations for hydraulic fracturing, exposure models for affected regions, and suggested nuisance risk thresholds adopted from previous studies on human discomfort to vibrations.

We have demonstrated and validated the proposed modelling approach, using the UK PNR shale gas site and its surrounding area as a test bed. In particular, we showed how the framework can be used to determine event magnitudes and injection volumes for which prescribed nuisance risk thresholds may be exceeded at buildings nearby the site. For the specific case study examined, in which seismic events were deterministically located close to the surface projection of the PNR well stimulated in late 2018, we found that ground motions equivalent in amplitude to that at which pile driving becomes perceptible may be exceeded in the location of at least one building for event magnitudes equal to or exceeding the current UK induced seismicity traffic light system ``red light'' event (i.e M_w = 1.1), or injection volumes $\geq$ 1000 m^3, while cosmetic damage may occur in

at least one building for $M_w \geq 2.1$ or injection volumes $\geq 40{,}000$ m^3. Future work will investigate the sensitivity of these results to modeling assumptions related to rupture behavior and the prediction of ground motion.

Finally, we discussed ways in which the proposed modelling approach could contribute to developing risk-informed policies for the management of induced seismicity related to UK shale gas exploration. For example, we suggested that the framework could be used to design an injection-volume-based traffic light system for induced seismicity, which would enable injection volumes to be controlled ahead of time to mitigate the probabilities of causing ground motions with nuisance risk potential. This proactive system could replace the reactive magnitude-based traffic light system currently used in the UK, in which the thresholds do not explicitly account for the associated risks. We expect the findings of this study to be helpful as a decision support tool for stakeholders involved in the regulation of shale gas exploration in the UK.

7. Acknowledgements

This work has been funded by the Natural Environment Research Council (NERC) Grant Number NE/R017956/1 ``Evaluation, Quantification and Identification of Pathways and Targets for the assessment of Shale Gas RISK (EQUIPT4RISK)", the Bristol University Microseismic Projects (BUMPS), and the British Geological Survey.

8. References

[1] Davies RJ, Foulger GR, Bindley A, Styles P (2013): Induced seismicity and hydraulic fracturing for recovery of hydrocarbons. *Marine and Petroleum Geology*, **45**, 171-185.

[2] Ellsworth WL (2013): Injection-induced earthquakes. *Science*, **341** (6142), 1225942.

[3] Kraft T, Mai PM, Wiemer S, Deichmann , Ripperger J, Kastli P, Bachmann C, Fah D, Wossner J, Giardini D. Enhanced geothermal systems: Mitigating risk in urban areas. *Eos, Transactions American Geophysical Union*, **90** (32), 273-274.

[4] Bommer JJ, Crowley H, Pinho R (2015): A risk-mitigation approach to the management of induced seismicity. *Journal of Seismology*, **19** (2), 623-646.

[5] Giardini D (2009): Geothermal quake risks must be faced. *Nature*, **462** (7275), 848.

[6] Macrae GA (2006): Decision making tools for seismic risk. *New Zealand Society of Earthquake Engineering Annual Conference, Napier, New Zealand.*

[7] Douglas J, Aochi H (2014): Using estimated risk to develop stimulation strategies for enhanced geothermal systems. *Pure and Applied Geophysics*, **171** (8), 1847-1858.

[8] Gupta A, Baker JW (2019): A framework for time-varying induced seismicity risk assessment, with application in Oklahoma. *Bulletin of Earthquake Engineering*, **17** (8), 4475-4493.

[9] Walters RJ, Zoback MD, Baker JW, Beroza GC (2015): Characterizing and responding to seismic risk associated with earthquakes potentially triggered by fluid disposal and hydraulic fracturing. *Seismological Research Letters*, **86** (4), 1110-1118.

[10] Foulger GR, Wilson MP, Gluyas JG, Julian BR, Davies RJ (2018): Global review of human-induced earthquakes. *Earth Science Reviews*, **178** , 438-514.

[11] Cornell CA (1968): Engineering seismic risk analysis. *Bulletin of the Seismological Society of America*, **58** (5), 1583-1606.

[12] Van Eck T, Goutbeek F, Haak H, Dost B (2006): Seismic hazard due to small-magnitude, shallow-source, induced earthquakes in the Netherlands. *Engineering Geology*, **87** (1-2), 105-121.

[13] Bommer JJ, Alarcon JE (2006): The prediction and use of peak ground velocity. *Journal of Earthquake Engineering*, **10** (1), 1-31.

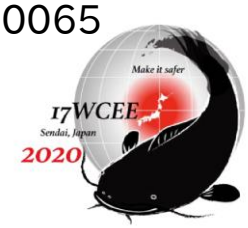

[14] Bommer JJ, Oates SJ, Cepeda JM, Lindholm C, Bird J, Torres R, Marroquin G, Rivas J (2006): Control of hazard due to seismicity induced by a hot fractured rock geothermal project. *Engineering Geology*, **83** (4), 287-306.

[15] Athanasopoulos G, Pelekis PC (2000): Ground vibrations from sheetpile driving in urban environment: measurements, analysis and effects on buildings and occupants. *Soil Dynamics and Earthquake Engineering*, **19** (5), 371-387.

[16] Barneich JA (1985): Vehicle induced ground motion. *Vibration Problems in Geotechnical Engineering*. ASCE

[17] BSI (1993): Evaluation and measurement for vibration in buildings: Guide to damage levels from groundborne vibration. *BS7385, British Standards Institute.*

[18] Ader T, Chendorain M, Free M, Saarno T, Heikkinen O, Malin PE, Leary P, Kwiatek G, Dresen G, Bluemle F, Vuorinen T (2019): Design and implementation of a traffic light system for deep geothermal well stimulation in Finland. *Journal of Seismology, (in press)*.

[19] Cuadrilla Resources Ltd. (2017): Preston New Road 1z Hydraulic Fracture Plan. *Report Commissioned by the Environment Agency, UK*

[20] Hallo M, Oprsal I, Eisner L, Ali, MY (2014). Prediction of magnitude of the largest potentially induced seismic event. *Journal of Seismology*, **18**(3), 421-431.

[21] Clarke H, Vedon JP, Kettlety T, Baird A, Kendall J-M (2019): Real-time imaging, forecasting, and management of human-induced seismicity at Preston New Road, Lancashire, England. *Seismological Research Letters*, **90** (5), 1902-1915.

[22] Hallo M, Eisner L, Ali MY (2012): Expected level of seismic activity caused by volumetric changes. *First Break*, **30** (7), 97-100.

[23] Mancini S, Segou M, Werner MJ, Baptie B (2019): Statistical modelling of the Preston New Road seismicity: Towards probabilistic forecasting tools. *Report No. CR/19/068 Commissioned by the Oil and Gas Authority.* Oil and Gas Authority, UK.

[24] Morris B, Medyckyj-Scott D, Burnhill P (2000): EDINA Digimap: new developments in the internet mapping and data service for the UK Higher Education community. *LIBER Quarterly*, **10** (4), 445-453.

[25] Cremen G, Werner MJ, Baptie B (2020): A new procedure for evaluating ground motion models, with application to hydraulic-fracture-induced seismicity in the UK. *Bulletin of the Seismological Society of America*, (in press).

[26] Haylock D (2001): *Numeracy for Teaching*. Sage.

[27] Bourne SJ, Oates SJ, Bommer JJ, Dost B, Van Elk J, Doornhof D (2015): A Monte Carlo method for probabilistic seismic hazard assessment of induced seismicity due to conventional natural gas production. *Bulletin of the Seismological Society of America*, **105** (3), 1721-1738.

[28] Musson RMW (1999): Determination of design earthquakes in seismic hazard analysis through Monte Carlo simulation approach. *Journal of Earthquake Engineering*, **3** (4), 463-474.

[29] Butcher A, Luckett R, Kendall J-M, Baptie B (2019): Corner frequencies, seismic moments and earthquake magnitudes: The effects of high-frequency attenuation on microseismicity. *Bulletin of the Seismological Society of America*, (in review).

[30] Grunthal G (1998): *European Macroseismic Scale 1998*. European Seismological Commission.

[31] BGS (2019): *Statement on Seismic Activity at Preston New Road, Lancashire on 28/8/19*. British Geological Survey.

[32] Cuadrilla Resources Ltd. (2019): Hydraulic Fracture Plan PNR 2. *Report Commissioned by the Environment Agency, UK.*

[33] Gallegos TJ, Varela BA, Haines SS, Engle MA (2015): Hydraulic fracture water use variability in the United States and potential environmental implications. *Water Resources Research*, **51** (7), 5839-5845

[34] Johnson EG, Johnson LA (2012): Hydraulic fracture water usage in northeast British Columbia: locations, volumes and trends. *Geoscience Reports 2012*. British Columbia Ministry of Energy and Mines.

